

THE OPTICAL MASS-LUMINOSITY RELATION AT THE END OF THE MAIN SEQUENCE (0.08–0.20 M_{\odot})¹

TODD J. HENRY

Harvard-Smithsonian Center for Astrophysics, Cambridge, MA 02138-1516; thenry@recons.harvard.edu

OTTO G. FRANZ AND LAWRENCE H. WASSERMAN

Lowell Observatory, Flagstaff, AZ 86001-4499; ogf, lhw@lowell.edu

G. FRITZ BENEDICT AND PETER J. SHELUS

Department of Astronomy, University of Texas, Austin, TX 78712-1083; fritz, pjs@astro.as.utexas.edu

PHILIP A. IANNA

Department of Astronomy, University of Virginia, Charlottesville, VA 22903-0818; pai@virginia.edu

J. DAVY KIRKPATRICK

IPAC, California Institute of Technology, Pasadena, CA 91125; davy@ipac.caltech.edu

AND

DONALD W. MCCARTHY, JR.

Department of Astronomy, University of Arizona, Tucson, AZ 85721-0065; mccarthy@as.arizona.edu

Received 1998 April 17; accepted 1998 September 25

ABSTRACT

The empirical mass-luminosity relation at M_V is presented for stars with masses 0.08–0.20 M_{\odot} based upon new observations made with Fine Guidance Sensor 3 on the *Hubble Space Telescope*. The targets are nearby, red dwarf multiple systems in which the magnitude differences are typically measured to ± 0.1 mag or better. The M_V values are generated using the best available parallaxes and are also accurate to ± 0.1 mag, because the errors in the magnitude differences are the dominant error source. In several cases this is the first time the observed sub-arcsecond multiples have been resolved at optical wavelengths. The mass-luminosity relation defined by these data reaches to $M_V = 18.5$ and provides a powerful empirical test for discriminating the lowest mass stars from high-mass brown dwarfs at wavelengths shorter than 1 μm .

Subject headings: astrometry — binaries: close — stars: low-mass, brown dwarfs — stars: luminosity function, mass function — stars: statistics — techniques: interferometric

1. INTRODUCTION

The dependence of intrinsic brightness upon mass, the mass-luminosity relation (MLR), is one of the few stellar relations sufficiently fundamental to be applicable to many areas of astronomy. With the exception of the H-R diagram, it is perhaps the single most important “map” of stellar astronomy, because the mass of a star is the key parameter that governs its entire evolution. For single objects, the MLR allows astronomers to convert a relatively easily observed quantity, luminosity, to a more revealing characteristic, mass, that yields a much better understanding of the nature of the object. In multiple systems revealed during astrometric, radial velocity, and cataclysmic binary work, astronomers use the MLR to estimate primary and secondary masses. In searches for extrasolar planets, the MLR provides masses for the target primary stars and permits companion detection limits to be set for both luminosity and mass. In the broader context of the Galaxy, an accurate MLR provides benchmarks for comparison to objects in stellar clusters, permits a luminosity function to be converted to a mass function, and drives estimates of the stellar contribution to the Galactic mass.

Despite its broad utility, the MLR remains poorly defined for M dwarfs, by far the dominant population of the

Galaxy in both numbers (> 70%) and stellar mass contribution (> 40%; Henry 1998). For red dwarfs with masses less than $\sim 0.2 M_{\odot}$, the MLR provides a direct empirical test of stellar evolutionary models, because an object’s luminosity is highly dependent upon age at such low masses. It takes roughly 0.2 Gyr for a 0.2 M_{\odot} star to reach the main sequence, but it takes 5 Gyr for a 0.08 M_{\odot} star (Burrows et al. 1993). To date, the effects of age on luminosity evident in the theoretical models of low-mass dwarfs remain empirically unchallenged. More importantly, below 0.1 M_{\odot} the MLR is critical for brown dwarf studies, because an accurate mass determination can convincingly turn a brown dwarf candidate into a bona fide brown dwarf.

Until the past decade, only four objects comprised our complete knowledge of the MLR for stars with $M \leq 0.2 M_{\odot}$ (Popper 1980). Substantial progress in defining the MLR has been made recently because of the development of high angular resolution techniques such as speckle imaging. This technique cleanly resolves multiple systems and allows orbits to be mapped so that the masses of the components can be determined. At optical wavelengths, very close binaries (separations $< 0''.1$) can be resolved, but optical speckle techniques are currently limited to relatively bright sources and/or shallow dynamic range, typically only a few mag. For low-mass binaries, infrared speckle imaging overcomes the faintness of the systems (low mass stars are brighter in the near-infrared than they are in the visible) and bridges the large dynamic range between a bright primary

¹ Based on observations with the NASA/ESA *Hubble Space Telescope* obtained at the Space Telescope Science Institute, which is operated by the Association of Universities for Research in Astronomy, Inc., under NASA contract NAS 5-26555.

and faint secondary. Henry & McCarthy (1993, hereafter HM93) used infrared speckle imaging to develop the first robust MLR for objects with masses less than $0.2 M_{\odot}$ by observing a sample of nearby binaries. They presented empirical relations in the near-infrared J , H , and K band-passes (1.2, 1.6, and $2.2 \mu\text{m}$, respectively) and provided 10 objects with masses less than $0.2 M_{\odot}$. For the first time, the MLR included objects falling near or in the stellar–brown dwarf transition region at $0.07\text{--}0.09 M_{\odot}$. However, direct measurements of the optical fluxes for the individual components in these systems were still unavailable.

We have been motivated to define the MLR at optical wavelengths, specifically, M_V in this paper, because much of our information about stars comes from large all-sky optical surveys. The M_V values for components in the low-mass multiple systems reported here have been determined with new observations made with Fine Guidance Sensor 3 (FGS3) on the *Hubble Space Telescope* (*HST*). Many of the systems observed have never before been resolved at optical wavelengths. When combined with the IR speckle work, the MLR has now been determined directly at wavelengths from 0.5 to $2.2 \mu\text{m}$ for objects near the end of the stellar main sequence.

2. SAMPLE

We have defined a list of multiple systems called the 20-20-20 sample, in which high-quality component masses

can be determined in a relatively short amount of time. Each system is within 20 pc, has an orbital period known to be shorter than 20 yr (but longer than 20 days to allow spatial resolution), and has at least one component with a mass less than 20% of the Sun. There are currently 16 such systems in the sample, all of which are listed in the top portion of Table 1.

Four more candidate systems listed in Table 1 are probable 20-20-20 sample members, but their orbital periods are currently unknown. Gl 487 ABC was first found to be a double-lined spectroscopic binary by Stauffer & Hartmann (1986). In 1989, one-dimensional infrared speckle measurements revealed Gl 487 to be a nearly equal magnitude double with a separation of a few tenths of an arcsecond, although the pair was not cleanly resolved. However, this speckle companion is not the same as that found by Stauffer & Hartmann (1986), thereby making the system triple, but no orbital information is yet available. The GJ 2005 ABCD system is now known to be a quadruple, given our discovery of component “D” during the *HST* FGS3 program (discussed further in § 3.3). Both the AD and BC doubles are sub-arcsecond binaries, and each double will likely meet the 20-20-20 sample criteria, although no orbital periods are yet known. The separation of AD-BC is only $\sim 1''.3$ (Leinert et al. 1994), so the data listed are for all four components. G89-32 AB and LHS 1885 AB were discovered to be binaries in 1996 April during an infrared speckle observing

TABLE 1
BASIC DATA FOR LOW-MASS MULTIPLE SYSTEMS

CNS Name	Other Name	B	V	R_C	I_C	Reference	J	H	K	L	Reference	Spectral Type	Reference
20-20-20 Sample Systems													
Gl 22 ABC	BD + 66 34	11.88	10.28	9.25	7.98	W96	M2 V	*
Gl 222 AB	χ^1 Ori	5.00	4.41	3.98	3.75	J68	3.30	3.01	2.95	2.89	J68	G0 V	CNS
Gl 234 AB	Ross 614	12.81	11.09	9.78	8.06	W96	6.38	5.78	5.49	5.33	L92	M4.5 V	*
Gl 469 AB	Wolf 414	...	12.06	10.87	9.33	*	M3.5 V	*
Gl 473 AB	Wolf 424	14.27	12.42	10.89	8.90	W96	6.96	6.39	6.06	...	L92	M5.5 V	*
Gl 494 AB	DT Vir	11.19	9.72	8.75	7.64	W96	6.46	5.80	5.61	5.40	L92	M1.5 V	*
Gl 623 AB	LHS 417	11.78	10.28	9.26	7.96	W96	6.67	6.14	5.91	...	L92	M2.5 V	*
Gl 748 AB	Wolf 1062	12.63	11.12	10.00	8.53	W96	7.08	6.55	6.31	6.05	L92	M3.5 V	*
Gl 791.2 AB	HU Del	14.72	13.06	11.72	9.96	L92	8.20	7.63	7.33	...	L92	M4.5 V	*
Gl 831 ABC	Wolf 922	13.66	11.98	10.69	9.00	W96	7.29	6.70	6.42	...	L92	M4.5 V	*
Gl 866 ABC	LHS 68	14.28	12.30	10.64	8.58	W96	6.50	5.91	5.57	5.22	L92	M5 V	*
GJ 1005 AB	LHS 1047	...	11.50	10.26	8.69	*	M4 V	*
GJ 1081 AB	G96-45	...	12.21	CNS	M3 V	*
GJ 1215 AB	LHS 3277	...	15.10	13.63	11.75	W96	M5.5 V	*
GJ 1245 AC	V1581 Cyg	...	13.41	11.82	9.79	W96	7.78	7.26	6.89	...	L92	M5.5 V	*
G250-29 AB	LHS 221	12.51	10.95	9.87	8.48	W96	M2.5 V	*
Probable 20-20-20 Sample Systems (unknown orbital periods)													
Gl 487 ABC	G237-78	12.54	10.91	9.79	8.32	L92	6.90	6.34	6.09	...	L92	M3 V	*
GJ 2005 ABCD	LHS 1070	...	15.42	13.71	11.56	L92	9.10	8.57	8.16	...	L92	M5.5 V	*
G89-32 AB	LTT 17993	...	13.22	11.80	9.94	W86	M4.5 V	*
LHS 1885 AB	G250-31	...	13.65	12.25	10.41	W96	M4.5 V	*
Additional Systems (orbital periods longer than 20 yr)													
Gl 53 AB	μ Cas	5.86	5.16	4.67	4.32	J68	3.81	3.36	3.34	3.31	J68	G5 VI	CNS
Gl 65 AB	LHS 9	13.86	11.99	10.36	8.30	W96	6.24	5.67	5.33	5.00	L92	M5.5 V + M6 V	*
Gl 166 BC ^a	40 Eri	12.82	11.19	9.95	8.32	L92	6.73	6.20	5.96	5.75	L92	M4.5 V	*
Gl 860 AB	Kruger 60	11.24	9.57	8.43	6.94	W96	5.56	4.97	4.71	4.48	L92	M3 V + M4 V	*

^a All data are for component C only.

REFERENCES.—(CNS) Gliese & Jahreiss 1991; (J68) Johnson et al. 1968; (L92) Leggett 1992; (W86) Weis 1986; (W96) Weis 1996; (*) RECONS program: see Henry, Kirkpatrick, & Simons 1994, Henry et al. 1997, Patterson et al. 1998.

run. G89-32 AB is the only system in the 20-20-20 sample without a trigonometric parallax, but Weis (1986) estimated the distance photometrically to be only 5.8 pc, under the assumption that G89-32 AB was a single object. Using infrared speckle imaging we have found the two components to be of nearly equal brightness at K ($2.2 \mu\text{m}$) with a separation of $\sim 0''.7$. The available photometric data combined with the infrared speckle resolution imply a distance of 9 pc for the system. Finally, LHS 1885 AB is listed as G250-31 "A" in the Yale Parallax Catalog (van Altena, Lee, & Hoffleit 1995), although no other information concerning its duplicity could be found.

Four additional systems not meeting the 20-20-20 sample criteria (all have $P > 20$ yr) are listed at the bottom of Table 1, because they add valuable information to the MLR: the systems contain secondaries with masses determined to be less than $0.20 M_{\odot}$. Of these systems, only Gl 65 AB has been observed with *HST* FGS3.

3. OBSERVATIONS

3.1. Photometry and Spectroscopy

Listed in Table 1 are data characterizing the systems in the 20-20-20 sample. System *BVRIJHKL* photometry has been collected from the literature, and missing data are being filled in during our own optical and infrared photometric programs, as described in Patterson, Ianna, & Begam (1998) and Henry et al. (1997), respectively. *BV* photometry is on the Johnson system, *RI* photometry is on the Cousins system, and *JHKL* photometry is on the CIT system. Many of the data have been taken from the extensive optical work of Weis (1996) and the compilation of optical/infrared photometry of Leggett (1992). *RI* photometry on the Kron system used by Weis has been converted to the Cousins system used by Leggett via relations for $(V-R)$ and $(V-I)$ colors based upon ~ 150 stars in common to the two studies, and given by

$$\begin{aligned} (V-R)_{\text{Leggett}} = & +0.073464(V-R)_{\text{Weis}}^2 \\ & + 0.450223(V-R)_{\text{Weis}} + 0.397860, \end{aligned} \quad (N = 151), \quad (1)$$

$$\begin{aligned} (V-I)_{\text{Leggett}} = & -0.033685(V-I)_{\text{Weis}}^2 \\ & + 1.081595(V-I)_{\text{Weis}} + 0.116277, \end{aligned} \quad (N = 156). \quad (2)$$

The two systems with G dwarf primaries have photometry in Johnson, MacArthur, & Mitchell (1968) that has been converted to the appropriate systems using calibrations in Leggett (1992). The only V photometry not available from these photometric studies or our own work, that of GJ 1081 AB, was taken from Gliese & Jahreiss (1991).

Also listed in Table 1 are spectral types for red dwarfs on the standard system of Kirkpatrick, Henry, & McCarthy (1991). These observations cover the wavelength range $\sim 5000\text{--}9500 \text{ \AA}$ at a resolution of $6\text{--}18 \text{ \AA}$. The combined types are given for all systems except Gl 65 AB, Gl 166 BC, and Gl 860 AB. For Gl 65 AB and Gl 860 AB, relatively large separations, small brightness ratios, and good seeing at the Multiple Mirror Telescope allowed the close binaries to be resolved and spectral types for each component to be determined: Gl 65 AB at $2''.3$ on 1990 January 20 and Gl 860 AB at $2''.5$ on 1990 September 13. The Gl 166 BC pair is

a wide binary with a semimajor axis of nearly $7''$ (Heintz 1974), so component C could be observed separately.

3.2. Magnitude Differences from *HST* FGS3

The low-mass multiples have been observed with *HST* FGS3 to measure separations, position angles, and magnitude differences through filter F583W. Here we discuss only the magnitude differences that will be used to develop the optical MLR; the astrometry is left to future papers when sufficient data are available to determine new high-quality orbits and masses for the components in the observed systems.

For the data discussed in this paper, *HST* FGS3 was used in the transfer function scan mode (TRANS). In this mode, the star selector mirrors in *HST* FGS3 move to scan the light of a binary star across a beam splitter, through a pair of orthogonal Koester's prisms (one for each axis, called X and Y), and onto photomultiplier tubes (PMTs). Typically, the instantaneous field of view moves $1 \text{ mas photon}^{-1}$ integration period. On each axis, the prism emits two interfering wave fronts (one from each side) that strike two different PMTs. The difference in counts between the two PMTs versus the tilt angle of the wave front at the entrance face of the Koester's prism yields the transfer function, referred to as the S curve. Usually, $20\text{--}80$ scans $0''.8\text{--}3''.0$ in length are made across a target. Each scan yields an S curve that is then cross-correlated and coadded to produce a high signal-to-noise ratio transfer function. During data analysis, binaries are deconvolved using S curves of single stars of appropriate color.

Illustrated in Figure 1 are the S curves along both axes for GJ 1245 AC on UT 1997 May 5. As is evident in the figure, in *HST* FGS3 the Y -axis S curve is significantly better than the S curve along the X -axis. In X , the measured separation is $0''.293$, and the magnitude difference is $\Delta F583W = 3.51$. In Y , the separation is $0''.531$, and the magnitude difference is $\Delta F583W = 3.29$. The $\Delta F583W$ value is measured independently in each axis, thereby providing a self-consistency check. The adopted value for $\Delta F583W$ for each observation is taken from the average of the two values from the two axes, in this case, $\Delta F583W = 3.40$.

The $\Delta F583W$ results from the *HST* FGS3 observations (if any) are given in Table 2 for the 20-20-20 sample systems as well as for the additional candidates and important systems as listed in Table 1. All observations made using *HST* FGS3 through 1998 June 30 (the nominal end of cycle 7) have been included. We list the total number of observations for which each system was clearly resolved (col. [3]) and the mean $\Delta F583W$ determined using those observations (col. [2]). The differences in the number of observations used and the total (col. [4]) reflect observations of systems in which the separation was less than 20 mas along one or both axes or when a third component was detected that could not clearly be resolved from the other two.

For Gl 473 AB the magnitude difference between the two components is nearly zero, and in three observations component B was measured to be slightly brighter than A. Component A has been chosen to be the southern component in the four observations to date (infrared speckle measurements show A to be consistently brighter than B in the infrared) and should remain so until ~ 2005 . In the cases of Gl 623 AB, Gl 791.2 AB, and GJ 1215 AB, consistent magnitude differences have not yet been reliably deter-

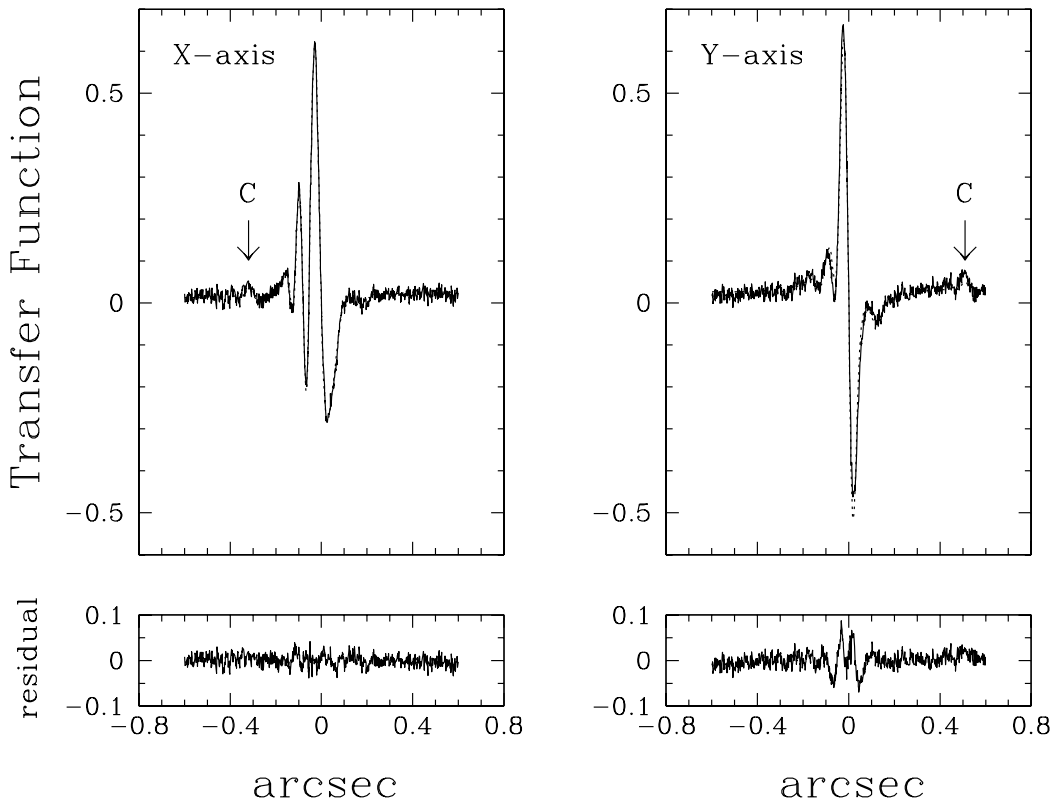


FIG. 1.—*HST* FGS3 TRANS results for GJ 1245 AC on UT 1997 May 5. The top two panels illustrate the S curves in the X and Y directions, each of which is the coaddition of 32 TRANS scans across the low-mass binary. The binary fits are shown with dotted lines, and the residuals are shown at the bottom. In both directions, the binary is clearly resolved, and component C is easily detected.

mined, because the companions are very close to their primaries and/or are very faint. Further analysis is required for these systems. G1 494 AB is the only system observed with *HST* FGS3 in which the companion has not been detected at all. The primary is relatively bright, and the companion is likely to be significantly fainter and very close (Heintz 1990) and therefore difficult to detect. Nevertheless, the astrometric orbit is convincing, and the system is worthy of further investigation with other techniques.

Column (2) of Table 2 contains the mean values of $\Delta F583W$ and the dispersions among the individual values, for which we adopt the standard deviations of the measurements when there are at least three observations. These dispersions are used rather than the formal errors in the mean, because they are more representative of our confidence in the mean values, given the likelihood of flaring of one or both components in these systems and the dependence of measurement accuracy upon the separation, which changes as the two components orbit one another. The three panels of Figure 2 illustrate the dependence of the dispersion in $\Delta F583W$ on system brightness, mean separation along each axis (as long as each is larger than 20 mas, the effective resolution limit of *HST* FGS3), and magnitude difference, with more challenging parameters toward the top of each panel. The dispersion is not clearly dependent on any of the system characteristics, although we would expect that it would be larger for fainter targets, decreasing separations, and increasing magnitude differences. What is clear is that for the 10 systems with three or more useful observations, the dispersion is never much more than 0.10 mag (except for GJ 2005 AD, which is a special case dis-

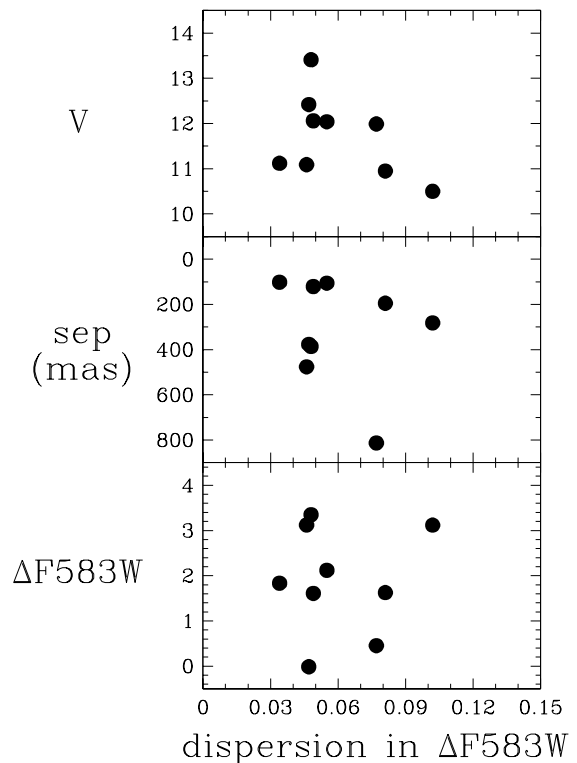


FIG. 2.—Observable parameters affecting dispersions in the measured $\Delta F583W$ values listed in Table 2. The dispersions are generally less than 0.10 mag and are independent of V magnitude, separation, and magnitude difference, at least throughout the ranges relevant to the present study.

TABLE 2
HST FGS3 OBSERVATIONS THROUGH 1998 JUNE 30

System (1)	Mean $\Delta F583W$ (2)	Number Used (3)	Number Total (4)	Notes (5)
20-20-20 Sample Systems				
Gl 22 AC	3.119 ± 0.102	4	4	
Gl 222 AB	0	0	Not observed
Gl 234 AB	3.122 ± 0.046	3	4	
Gl 469 AB	1.610 ± 0.049	4	4	
Gl 473 AB	-0.013 ± 0.047	4	4	
Gl 494 AB	0	2	Unresolved
Gl 623 AB	0	15	Pending
Gl 748 AB	1.834 ± 0.034	14	18	
Gl 791.2 AB.....	...	0	15	Pending
Gl 831 AB-C.....	2.9 ± 0.3	2	12	C Resolved
Gl 831 AB	2.120 ± 0.055	8	12	AB Resolved
Gl 866 AC-B.....	0.402 ± 0.100^a	1	1	B Resolved
Gl 866 AC	0	1	AC Not resolved
GJ 1005 AB.....	...	0	16	Other program
GJ 1081 AB.....	1.684 ± 0.100^a	1	1	
GJ 1215 AB.....	...	0	4	Pending
GJ 1245 AC.....	3.349 ± 0.048	3	3	
G250-29 AB.....	1.627 ± 0.081	3	4	
Probable 20-20-20 Sample Systems				
Gl 487 ABC.....	...	0	0	Not observed
GJ 2005 AD	2.513 ± 0.256	3	4	
G89-32 AB	0	0	Not observed
LHS 1885 AB.....	...	0	0	Not observed
Additional Systems				
Gl 53 AB	0	0	Not observed
Gl 65 AB	0.455 ± 0.077	15	15	
Gl 166 BC	0	0	Not observed
Gl 860 AB	0	0	Not observed

^a Fewer than three observations; dispersion estimated.

cussed in § 3.3). For the Gl 866 ABC and GJ 1081 AB systems in Table 2, which have only one observation each, we therefore make a conservative estimate of 0.10 mag in the error for the $\Delta F583W$ value.

Additional factors contributing to the consistency of $\Delta F583W$ measurements include the mismatch in color between the components fit in the TRANS analysis and the stars used to generate the calibration S curves and true variability in the stars themselves. Many of the components in these systems are flare stars, e.g., Gl 65 AB is UV Ceti, so the magnitude differences may exhibit real fluctuations.

3.3. New Low-Mass Companions with *HST* FGS3

During the course of the *HST* FGS3 work, two systems have revealed additional components that were previously unknown, Gl 831 C and GJ 2005 D.

As reported by Franz et al. (1997), Gl 831 was resolved into three components twice in the first 11 observations. The faint tertiary “C” is approximately 3 mag fainter than the primary (measured $\Delta F583W$ values are 2.8 and 3.6) and is likely variable. It is either very close to A or B (the A-B separation is $\sim 0''.14$) or more than $0''.5$ distant, beyond the typical *HST* FGS3 scan length for this system. Magnitude differences for both A-B and AB-C are listed in Table 2. Additional *HST* FGS3 observations of this intriguing system are planned.

Only a few years ago, GJ 2005 (LHS 1070) was found to be triple, with two companions lying $1''.3$ from the primary (Leinert et al. 1994). Our *HST* FGS3 measurements have revealed a fourth component only ~ 50 mas from component A that exhibits rapid orbital motion. This component “D” has been detected in all four *HST* FGS3 observations to date and has $\Delta F583W = 2.2\text{--}2.8$. It appears that the wide companions, B and/or C, have been detected by *HST* FGS3 as additional sources in three of the four observations to date, although at $V \sim 19$ for each, the signatures in the S curves are very weak.

4. DATA ANALYSIS

4.1. Conversion of $\Delta F583W$ to ΔV

The F583W aperture in *HST* FGS3 was selected for the observations because it nearly matches the Johnson V band and is currently the best calibrated of the filters available in *HST* FGS3. The effective wavelength is 5830 Å, and the FWHM is 2340 Å. The transformation of F583W magnitudes to the Johnson V band has been calibrated using 588 measurements of 92 stars in M35 (Bucciarelli et al. 1994), and it is given by

$$V = F583W + 20.060 - 0.164(B - V). \quad (3)$$

For the present purposes, we are concerned with the magnitude difference between two components in a binary,

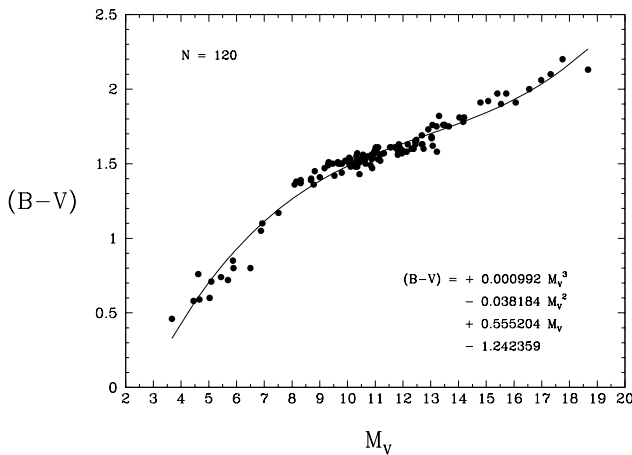


FIG. 3.—Relation $(B-V)$ vs. M_V for nearby, main-sequence stars that have no known close companions. The least-squares polynomial fit illustrated is used in the conversion from the measured $\Delta F583W$ to ΔV , as discussed in the text.

ΔV , which can be derived from equation (3) and is given by

$$\Delta V = \Delta F583W + 0.164[(B-V)_A - (B-V)_B]. \quad (4)$$

Therefore, to convert $\Delta F583W$ to ΔV requires knowledge of the $(B-V)$ colors of the individual components in a multiple. We can use the V magnitudes for the combined systems, the parallaxes, and the magnitude differences, $\Delta F583W$, to estimate *approximate* M_V values for the com-

ponents. These M_V values can then be used to estimate individual $(B-V)$ values for each component via the relation shown in Figure 3 and described by

$$(B-V) = +0.000992M_V^3 - 0.038184M_V^2 + 0.555204M_V - 1.242359. \quad (5)$$

The 120 stars used to generate this fit are all within 10 pc of the Sun, (thereby having high-quality parallaxes), are not known to have any companions that corrupt the photometry, and are not white dwarfs. The difference in the $(B-V)$ values for the two components then provides the final adjustment from $\Delta F583W$ to ΔV . For a given system, the total error in the adjustment includes errors in (1) the parallax (these affect the M_V estimate for the stars in the target binary); (2) the V magnitude; (3) the measured $\Delta F583W$ values of Table 2; (4) the error in the coefficient, 0.164 ± 0.010 , of equation (4); and (5) the rms scatter about the fit. The last error dominates the others and is caused by errors in M_V for the 120 stars shown in Figure 3 and the unavoidable differences in their ages and metallicities. The rms scatter is 0.0591 mag in $(B-V)$, and is added in quadrature for each component's $(B-V)$ value used in equation (4). The final adjustment from $\Delta F583W$ to ΔV is 0.06 mag or less in all of the cases considered.

A note of caution is in order. In many cases we know that the companions are red because we have also resolved them at infrared wavelengths. However, Gl 469 B, Gl 831 C, GJ 1081 B, and GJ 2005 D have not been resolved at infrared wavelengths, so we cannot be certain that the companions

TABLE 3
PARALLAXES, ΔV , M_V AND REVISED MASSES FOR LOW-MASS MULTIPLE SYSTEMS

SYSTEM	π_{trig}	REFERENCE	V	ΔV^a	M_V		REVISED MASS		
					Primary	Secondary	M_A	M_B	
Systems observed with <i>HST</i> FGS3									
Gl 22 AC ^b	0.0998 ± 0.0025	Y	10.50 ± 0.04^c	3.08 ± 0.10	10.56 ± 0.07	13.64 ± 0.12	0.361 ± 0.039	0.128 ± 0.014	
Gl 65 AB	0.3737 ± 0.0027	Y	11.99 ± 0.03	0.45 ± 0.08	15.40 ± 0.05	15.85 ± 0.06	0.102 ± 0.010	0.100 ± 0.010	
Gl 234 AB	0.24289 ± 0.00264	H	11.09 ± 0.03	3.08 ± 0.05	13.08 ± 0.04	16.16 ± 0.06	0.178 ± 0.047	0.083 ± 0.023	
Gl 469 AB	0.07377 ± 0.00367	H	12.06 ± 0.05	1.59 ± 0.05	11.63 ± 0.12	13.22 ± 0.13	
Gl 473 AB	0.2279 ± 0.0046	Y	12.42 ± 0.03	-0.01 ± 0.05	14.97 ± 0.06	14.96 ± 0.06	
Gl 623 AB	0.12434 ± 0.00116	H	10.28 ± 0.03	5.28 ± 0.10^d	10.76 ± 0.04	16.04 ± 0.11	0.608 ± 0.212	0.136 ± 0.050	
Gl 748 AB	0.0998 ± 0.0024	Y	11.12 ± 0.03	1.81 ± 0.04	11.30 ± 0.06	13.11 ± 0.07	
Gl 831 AB-C ^{b,e}	0.1258 ± 0.0023	Y	11.98 ± 0.03	2.9 ± 0.3	...	15.4 ± 0.2	
Gl 831 AB	0.1258 ± 0.0023	Y	12.06 ± 0.03	2.10 ± 0.06	12.70 ± 0.05	14.80 ± 0.07	
Gl 866 AC-B ^{b,e}	0.2895 ± 0.0044	Y	12.30 ± 0.03	0.40 ± 0.10	...	15.58 ± 0.07	
Gl 866 AC	0.2895 ± 0.0044	Y	12.85 ± 0.05	Unknown	
GJ 1081 AB	0.0652 ± 0.0018	Y	12.21 ± 0.05	1.67 ± 0.10	11.49 ± 0.08	13.16 ± 0.11	
GJ 1245 AC	0.2202 ± 0.0010	Y	13.41 ± 0.03	3.29 ± 0.05	15.18 ± 0.03	18.47 ± 0.06	0.129 ± 0.021	0.074 ± 0.013	
GJ 2005 AD ^b	0.1353 ± 0.0121	Y	15.50 ± 0.09^f	2.46 ± 0.26	16.26 ± 0.22	18.72 ± 0.32	
G250-29 AB	0.09402 ± 0.00218	H	10.95 ± 0.03	1.61 ± 0.08	11.04 ± 0.06	12.65 ± 0.09	
Additional components with masses known to be less than $0.20 M_{\odot}$									
Gl 166 C	0.19824 ± 0.00084	H	11.19 ± 0.03^g	12.68 ± 0.03	...	0.177 ± 0.029	
Gl 860 B	0.24952 ± 0.00303	H	9.57 ± 0.03	1.61 ± 0.06^h	...	13.39 ± 0.06	...	0.172 ± 0.008	

NOTE.—Parallaxes and errors have been taken from (Y) the Yale Parallax Catalog (van Altena et al. 1995) and (H) the *Hipparcos* mission (ESA 1997).

^a Converted from $\Delta F583W$ as described in the text.

^b Additional components complicate V magnitude deconvolution.

^c AC-B deconvolved with *Hipparcos* $\Delta \text{mag} = 1.63 \pm 0.10$.

^d From Barbieri et al. (1996).

^e Deconvolution of close pair and distant tertiary accomplished with $\Delta F583W$ from *HST* FGS3.

^f V magnitude for AD from C. Leinert (1998, private communication).

^g Component C only.

^h AB deconvolved with *Hipparcos* $\Delta \text{mag} = 1.61 \pm 0.06$.

are red dwarfs and not white dwarfs. Nonetheless, it is unlikely that these companions are white dwarfs given that estimates of the total mass in these systems are much too low to allow for white dwarfs with masses of $0.5 M_{\odot}$ or more to be present.

4.2. New M_V Values and Revised Masses

In Table 3 we list the systems observed with *HST* FGS3 (and two additional important components) and summarize the information required to derive M_V values. The parallaxes and their errors have been taken from the Yale Parallax Catalog (van Altena et al. 1995) and the *Hipparcos* mission (ESA 1997), referenced as Y and H, respectively. If both sources had parallax determinations, the one with the lower error was selected. The V photometry is from Table 1. The magnitude differences listed, ΔV , have been derived from the measured $\Delta F583W$ as described in the previous section. For comparison, the value of $\Delta V = 0.84$ found by Rakos et al. (1982) for Gl 65 AB, and that derived by Geyer, Harrington, & Worley (1988), $\Delta m_{\text{phot}} = 0.76$, are larger than our value of $\Delta V = 0.45 \pm 0.08$. However, our value matches the 0.4–0.5 mag difference reported by visual observers, and the consistency of the 15 observations made with *HST* FGS3 to date favors the smaller magnitude difference. In a more difficult case, we have adopted $\Delta V = 5.28 \pm 0.10$ for Gl 623 AB from Barbieri et al. (1996), who observed the system once through filter F486N with the Faint Object Camera on *HST*. We have derived ΔV from the V magnitude for the system and their V magnitude for Gl 623 B ($V = 15.57$). The system is exceptionally challenging for *HST* FGS3 because of the large magnitude difference and close separation. Component B has been detected in many of the *HST* FGS3 observations to date, but we await a rigorous photometric/astrometric analysis before reporting a ΔV value.

The parallaxes given are the highest quality currently available and lead to revisions of estimated M_V values in HM93 even without the new *HST* FGS3 measurements. They also lead to slight adjustments in masses for the seven systems in HM93 for which full dynamic elements have been derived. Consequently, new masses for these systems have been calculated and are also given in Table 3. *No mass revisions due to orbital refinement have been included in these mass determinations.* The current orbital coverage for the low-mass binaries is insufficient to warrant a rederivation of the component masses at this time. However, in a few more years several of the systems described will have more than half of their orbits mapped accurately through the combination of *HST* FGS3/FGS1R and infrared speckle efforts. FGS1R is a refurbished FGS with on-board adjustments to maximize the quality of interferometer response functions on both axes. It was installed during the servicing mission in 1997 February, and the plan is to begin using it for scientific observations in cycle 8.

5. DISCUSSION

5.1. History of the MLR from 0.08 to $0.20 M_{\odot}$ at Optical Wavelengths

In 1980, the MLR near the end of the main sequence included only four stars with $M \leq 0.2 M_{\odot}$ (Popper 1980), Gl 65 A, Gl 65 B, Gl 166 C, and Gl 860 B. The reason for the paucity of accurate M dwarf mass determinations is that these small stars seldom present orbits in which they eclipse,

so visual binaries must be used. In order to have reliable orbits, the visual systems must have small separations in order to complete orbits in timescales measured in yr rather than centuries. Consequently, these close orbits make clear resolution of the pairs difficult from the ground, a problem compounded by the fact that these low-mass systems are faint, even when nearby.

The small sample of very low mass stars in Popper (1980) was increased to a dozen by Liebert & Probst (1987), but four of those 12 had crude mass estimates subject to orbital assumptions (Gl 473 A, Gl 473 B, Gl 748 B, and Gl 896 B), and one had a subdwarf primary and is thus presumably a subdwarf itself (Gl 53 B). The remaining seven points included only three new objects—Gl 234 A, Gl 234 B, and Gl 623 B. Their mass estimates relied upon preliminary infrared speckle analyses, and the systems had not been resolved reliably at optical wavelengths. The two studies of Harmanec (1988) and Andersen (1991) showed progress in the MLR for stars more massive than $0.2 M_{\odot}$, but neither added any stars at lower masses. Although HM93 made a first attempt at the MLR below $0.2 M_{\odot}$ at optical wavelengths, they relied upon an empirical ($V-K$) versus M_K relation to estimate M_V for components in systems that had been resolved with infrared speckle imaging. The resulting MLR can now be improved using the direct measurements at optical wavelengths made with *HST* FGS3.

5.2. The New MLR from 0.08 to $0.20 M_{\odot}$ at Optical Wavelengths

Shown in Figure 4 is the empirical MLR at M_V for objects with masses 0.08– $0.20 M_{\odot}$. The results in Table 3 and illustrated in Figure 4 supersede those in HM93. Objects with ΔV measured by *HST* FGS3 are shown with solid circles. The three stars with ΔV not measured with *HST* FGS3 are shown as triangles. Open circles represent the locations of the same points in the M_V -mass relation of HM93 before the *HST* FGS3 measurements and new parallaxes. The Gl 352 system, in which both components were reported to have masses near $0.20 M_{\odot}$ in HM93, now has an improved parallax from *Hipparcos*, $\pi_{\text{trig}} = 0.09495 \pm 0.00431$. This places both components well above the $0.20 M_{\odot}$ limit of concern in this paper, at 0.29 and $0.30 M_{\odot}$.

The shaded region in Figure 4 delineates the main-sequence minimum mass (MSMM) range for dwarfs with metallicities ranging from zero ($0.092 M_{\odot}$, Saumon et al. 1994) to the most recent solar models ($0.072 M_{\odot}$, Chabrier & Baraffe 1997). Both sets of models have helium fractions appropriate to the Sun, $Y = 0.25$. In general, increasing the helium fraction or metallicity decreases the resulting MSMM. Although the models have increased in sophistication—with improved interior physics, opacity source contributions, and nongray atmospheric effects—these values are only slightly different than earlier determinations of the MSMM at $\sim 0.08 M_{\odot}$ (D’Antona & Mazzitelli 1985; Nelson, Rappaport, & Joss 1986) and 0.074 – $0.098 M_{\odot}$ (Burrows et al. 1993). In fact, Kumar (1963) reported that “for stars with Population I composition, the limiting mass is approximately 0.07. Similarly, for the Population II stars the limiting mass is approximately 0.09.” The MSMM range as plotted therefore represents confident limits of the stellar–brown dwarf transition region, given that the values have not changed in 35 yr.

Illustrated with a dotted curve is the MLR fit from HM93 (their Fig. 2 and eq. 5c) for the lower main sequence at M_V ,

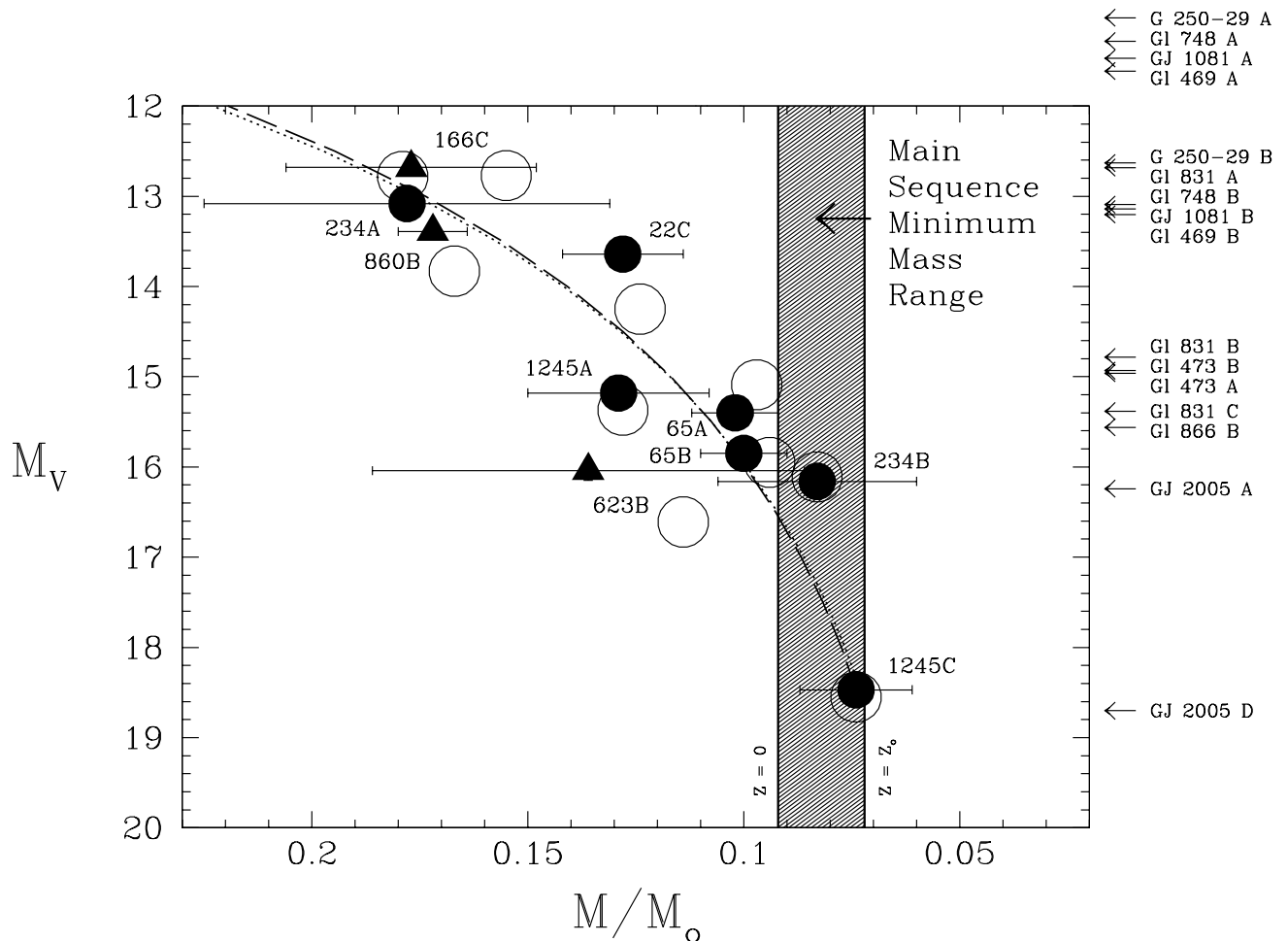


FIG. 4.—Optical mass-luminosity relation at the end of the main sequence. The shaded region with borders at 0.092 and $0.072 M_{\odot}$ marks the main-sequence minimum mass range for objects with zero to solar metallicity. Solid circles are targets in the 20-20-20 sample that have been clearly resolved by *HST* FGS3. The three stars represented by triangles have not been observed (Gl 166C and Gl 860B) or await further analysis (Gl 623B). Large open circles represent the same objects as the filled symbols at the M_V values given in HM93. Points have shifted because of improved ΔV values from the *HST* work and new parallaxes. The two curves are the 1993 fit (dotted line) and the new fit (dashed line) generated with the data presented here. Objects on the right are being observed with *HST* and are plotted at their M_V values, but no reliable masses are yet available.

given by

$$\log(M/M_{\odot}) = +0.005257M_V^2 - 0.2351M_V + 1.4124 \quad (\text{Old}). \quad (6)$$

Given the new parallaxes and *HST* FGS3 measurements, it is possible to make an improved fit to the 10 data points, represented by a dashed curve and given by

$$\log(M/M_{\odot}) = +0.005239M_V^2 - 0.2326M_V + 1.3785 \quad (\text{New}). \quad (7)$$

It is reassuring that the HM93 relation and this new relation are so similar, indicating that the methodology used to estimate M_V values in HM93 was sound. The M_V estimates in HM93 relied upon infrared photometry, infrared speckle measurements, parallaxes from Gliese & Jahreiss (1991), and color-magnitude relations [e.g., $(V-K)$ vs. M_K], each of which had its own associated errors. Given these error sources, particularly the spread in the color-magnitude relations (with rms scatters of 0.25 – 0.30 mag), it is not surprising that the points have shifted somewhat from their earlier values (Fig. 4, open circles).

Recent theoretical models for low-mass stars by Baraffe et al. (1998) predict a spread in M_V of 0.5 – 1.0 mag for stars with masses 0.08 – $0.20 M_{\odot}$ when considering a metallicity range from $[M/H] = 0$ to -0.5 . Therefore, even if the mass errors were greatly reduced for the stars plotted in Figure 4, we would expect some vertical offsets in M_V values. As mentioned earlier, the effects of age will also lead to a spread for the points, and it is precisely the effects of age and metallicity on the MLR near the end of the main sequence that we hope to investigate in the future, when more and higher quality masses have been determined.

5.3. Imminent Progress in the MLR from 0.20 to $0.50 M_{\odot}$

The MLR between 0.20 and $0.50 M_{\odot}$ is perhaps more poorly defined than at lower masses. In this mass regime, the effects of H_2 molecules forming in the stellar atmosphere and a deepening convective region combine to produce a plateau in the MLR, so that there is little change in flux with mass. The result is virtually a scatter diagram of only a few points, many of them of low quality. Fortunately, the infrared speckle and *HST* FGS3/FGS1R program will improve the situation markedly. Several of the primaries included in the 20-20-20 sample—Gl 469 A, Gl 748 A, GJ

TABLE 4
MASS ESTIMATES FOR VERY LOW
MASS OBJECTS OBSERVED WITH
HST FGS

Name	M_V	Mass
GI 469 A	11.63	0.24
GI 469 B	13.22	0.17
GI 473 A	14.97	0.12
GI 473 B	14.96	0.12
GI 748 A	11.30	0.26
GI 748 B	13.11	0.17
GI 831 A	12.70	0.19
GI 831 B	14.80	0.12
GI 831 C	15.4	0.11
GI 866 B	15.58	0.11
GJ 1081 A	11.49	0.25
GJ 1081 B	13.16	0.17
GJ 2005 A	16.26	0.10
GJ 2005 D	18.72	0.07
G250-29 A	11.04	0.28
G250-29 B	12.65	0.19

1081 A, and G250-29 A—will have masses determined for the first time, while others, e.g., GI 22 A, will have improved masses.

5.4. Mass Estimates for Members of the 20-20-20 Sample

Although the MLR in Figure 4 is an improvement on what was presented in HM93 at optical wavelengths, we can look forward to the addition of several more systems in the next few years. Shown on the right-hand side of Figure 4 are components of 20-20-20 sample systems included in *HST* FGS3 programs led by the authors that do not yet have reliable mass determinations. The new MLR allows us to predict masses for these objects, and these are listed in Table 4. Although only approximate, these mass estimates serve as guidelines to direct efforts toward the most important systems.

6. FUTURE

The 10 objects with dynamically determined masses less than $0.2 M_{\odot}$ in the current MLR have mass errors of 4%–37%, with only one, GI 866 B, having an error much less than 10%. Obviously, there is much progress yet to be made in determining the MLR at the end of the main sequence.

Our observational goal is to map the relative orbits of the low-mass systems in the 20-20-20 sample through a coordi-

nated program of *HST* FGS3/FGS1R observations and ground-based infrared speckle work. Currently, the mass errors in these systems are dominated by uncertain *relative* orbit semimajor axes (5%–10%) because of the limited precision of the ground-based speckle observations, typically 10–50 mas. A 10-fold improvement in the accuracy of the separation measurements, to 2 mas, has been demonstrated with *HST* FGS3 in TRANS mode for the GI 748 system (Franz et al. 1998). For a given binary, this yields an orbital semimajor axis that is accurate to <1%, which typically translates into a reduction in the mass errors to $\sim 3\%$, because the semimajor axis error enters as a cubed term in the mass determinations. In addition, we anticipate that new mass determinations for systems in the 20-20-20 sample will yield an increase in the number of points in the low-mass MLR from 10 to ~ 20 by the year 2000. (12 of 16 of the objects shown on the right-hand side of Fig. 4 have mass estimates less than $0.2 M_{\odot}$.) Finally, radial velocity work in a concerted effort at the Hobby-Eberly Telescope in Texas will allow us to improve the orbital elements further.

The combination of high-quality masses and an increased sample will allow the effects of age and metallicity on the MLR to be mapped for objects with masses less than $0.2 M_{\odot}$. These are important objects to study, because they account for a full third of solar neighborhood members. In addition, two of the objects in the 20-20-20 sample, GI 234 B and GJ 1245 C, currently have masses determined to straddle the stellar–brown dwarf border, with $M = 0.082 \pm 0.023$ and $0.074 \pm 0.013 M_{\odot}$, respectively. These are the lowest mass objects for which dynamical masses have been determined. Improved masses will reveal whether they and new low-mass companions such as GJ 2005 D are, in fact, stars or brown dwarfs.

We thank Denise Taylor and Jack MacConnell for their tireless efforts that made this *HST* observational program possible. Support for this work was provided by NASA through grants GO-06047.03-94A, GO-06566.03-95A, and GO-07493.01-96A from the Space Telescope Science Institute, which is operated by the Association of Universities for Research in Astronomy, Inc., under NASA contract NAS 5-26555. T. J. H. received additional support from NASA through Hubble Fellowship grant HF-1058.01-94A, also from STScI. Members and associates of the Space Telescope Astrometry Team received additional support from NASA under grant NAG 5-1603 awarded to the University of Texas.

REFERENCES

- Andersen, J. 1991, *A&A Rev.*, 3, 91
 Baraffe, I., Chabrier, G., Allard, F., & Hauschildt, P. H. 1998, *A&A*, 337, 403
 Barbieri, C., DeMarchi, G., Nota, A., Corrain, G., Hack, W., Ragazzoni, R., & Macchetto, D. 1996, *A&A*, 315, 418
 Bucciarelli, B., Holfeltz, S. T., Lattanzi, M. G., Taff, L. G., & Vener-Saavedra, P. C. 1994, *PASP*, 106, 417
 Burrows, A., Hubbard, W. B., Saumon, D., & Lunine, J. I. 1993, *ApJ*, 406, 158
 Chabrier, G., & Baraffe, I. 1997, *A&A*, 327, 1039
 D'Antona, F., & Mazzitelli, I. 1985, *ApJ*, 296, 502
 ESA. 1997, *The Hipparcos and Tycho Catalogues*, (ESA SP-1200) (Noordwijk: ESA)
 Franz, O. G., et al. 1998, *AJ*, 116, 1432
 ———. 1997, *BAAS*, 191, 9302
 Geyer, D. W., Harrington, R. S., & Worley, C. E. 1998, *AJ*, 95, 1841
 Gliese, W., & Jahreiss, H. 1991, *Preliminary Version of the Third Catalog of Nearby Stars (NSSDC/ADC Cat. 5070A)* (Greenbelt, MD: GSFC)
 Harmanec, P. 1988, *Bull. Astron. Inst. Czechoslovakia*, 39, 329
 Heintz, W. D. 1990, *AJ*, 99, 420
 ———. 1974, *AJ*, 79, 819
 Henry, T. J. 1998, in *ASP Conf. Ser. 134, Brown Dwarfs and Extrasolar Planets*, ed. R. Rebolo, E. L. Martin, & M. R. Zapatero Osorio (San Francisco: ASP), 28
 Henry, T. J., Ianna, P. A., Kirkpatrick, J. D., & Jahreiss, H. 1997, *AJ*, 114, 388
 Henry, T. J., Kirkpatrick, J. D., & Simons, D. A. 1994, *AJ*, 108, 1437
 Henry, T. J., & McCarthy, D. W., Jr. 1993, *AJ*, 106, 773
 Johnson, H. L., MacArthur, J. W., & Mitchell, R. I. 1968, *ApJ*, 152, 465
 Kirkpatrick, J. D., Henry, T. J., & McCarthy, D. W., Jr. 1991, *ApJS*, 77, 417
 Kumar, S. S. 1963, *ApJ*, 137, 1121
 Leggett, S. K. 1992, *ApJS*, 82, 351
 Leinert, C., Weitzel, N., Richichi, A., Eckart, A., & Tacconi-Garman, L. E. 1994, *A&A*, 291, L47
 Liebert, J., & Probst, R. G. 1987, *ARA&A*, 25, 473
 Nelson, L. A., Rappaport, S. A., & Joss, P. C. 1986, *ApJ*, 311, 226

- Patterson, R. J., Ianna, P. A., & Begam, M. C. 1998, AJ, 116, 1132
Popper, D. M. 1980, ARA&A, 18, 115
Rakos, K. D., et al. 1982, A&AS, 47, 221
Saumon, D., Bergeron, P., Lunine, J. I., Hubbard, W. B., & Burrows, A.
1994, ApJ, 424, 333
Stauffer, J. R., & Hartmann, L. W. 1986, ApJS, 61, 531
- van Altena, W. F., Lee, J. T., & Hoffleit, E. D. 1995, The General Catalogue
of Trigonometric Stellar Parallaxes (4th ed.; New Haven: Yale Univ.
Obs.)
Weis, E. W. 1986, AJ, 91, 626
———. 1996, AJ, 112, 2300